Int. J. Heat Mass Transfer. Vol. 31, No. 12, pp. 2527–2541, 1988
Printed in Great Britain

0017–9310/88 $3.00 + 0.00

Combined convection from an isothermal horizontal rod buried in a porous medium

H. M. BADR
Mechanical Engineering Department, King Fahd University of Petroleum and Minerals, Dhahran 31261, Saudi Arabia

and

I. POP
Faculty of Mathematics, University of Cluj, Cluj, CP 253, Romania

(*Received* 19 *March* 1987 *and in final form* 3 *March* 1988)

Abstract—This paper reports the results of a numerical investigation of mixed convection heat transfer from a horizontal rod of circular cross-section that is embedded in a porous medium. The rod temperature is first assumed to be the same as that of the medium and then suddenly increased to a higher constant value. The steady-state problem has been solved by the method of series truncation in combination with a finite-difference scheme for the two flow configurations of parallel and counter-flow regimes. The flow and thermal fields as well as the variations of the average and local heat transfer rates with a wide range of Reynolds number, Grashof number and buoyancy parameter have been examined in detail for a Prandtl number of 0.7. One of the interesting features found is the occurrence of a recirculating flow zone near the upper half surface of the rod in the case of the counter-flow regime. The numerical method and the results presented fill in a gap in the literature on one of the most fundamental problems in the field of mixed convection in porous media.

1. INTRODUCTION

INTENSIVE interest has been shown in recent years in the area of convective heat transfer in fluid-saturated porous media. This is quite natural because of the numerous and wide-ranging engineering applications of convective flow through porous media. For example, this class of phenomena is encountered in industrial and geophysical contexts such as petroleum reservoir modelling, thermal insulation techniques, geothermal activities, chemical and nuclear engineering, solar power collectors, regenerative heat exchangers containing porous materials, burying of drums containing heat generating chemicals in the earth and underground spread of pollutants. Bejan [1], Cheng [2] and Nield [3] have recently provided extensive state-of-the-art reviews on convective heat transfer in fluid-saturated porous media.

One of the most basic problems in porous media which has important applications to the design of canisters for nuclear waste disposal systems is the natural convection from a horizontal circular cylinder embedded in a porous medium. Schrok *et al.* [4] and Fernandez and Schrok [5] have carried out experiments and numerical calculations for a cylinder buried beneath a permeable, horizontal surface. Their work resulted in a heat transfer correlation fitting the determined experimental and numerical data within a standard deviation of 11.4%. Unsteady heat transfer from a circular cylinder immersed in a porous medium through which a liquid is flowing according to Darcy's law in a potential flow has been studied by Sano [6]. He derived asymptotic solutions for large and small Peclet numbers, Pe, for the case where the unsteady temperature field is produced by a step change in wall temperature. The former solution is valid for $Pe > 200$ and the latter one for $Pe < 0.1$, respectively. The series solution for small time, which is valid for all values of Pe, is first obtained. Euler's transformation is then applied to the series solution for the average Nusselt number resulting in improving the convergence criterion as well as giving satisfactory results for most values of time. Similarity solutions of the governing equations that describe the steady natural convection about a circular cylinder in a porous medium were obtained by Merkin [7], Nilson [8] and recently by Fand *et al.* [9], who relied on the framework provided by the boundary-layer theory. In ref. [9] the authors have also presented interesting experimental results for porous media consisting of randomly packed glass spheres saturated by either water or silicone oil. More recently, the cylinder geometry was the subject of a detailed numerical study [10], which obtained, at large Rayleigh numbers, the second-order boundary-layer solution, too. Ingham *et al.* [11] have reported analytical and numerical solutions for the time-dependent natural convection boundary layer due to sudden imposition of a temperature difference between the cylinder surface and the fluid-saturated medium.

Despite the strong interest expressed by the fluid mechanics community in the problem of mixed con-

NOMENCLATURE

a	radius of the rod
g	gravitational acceleration
Gr	modified Grashof number
$h, \bar{h}$	local and average heat transfer coefficients
k	fluid–porous matrix conductivity
K	porous medium permeability
$Nu, \overline{Nu}$	local and average Nusselt numbers
Pr	Prandtl number
q	heat transfer rate
r	dimensionless radial coordinate
Re	Reynolds number, $2au_\infty/\nu$
t	dimensionless time
T	dimensional temperature
u_∞	free stream velocity
v_r, v_θ	Darcian dimensionless radial and transverse components of velocity.

Greek symbols

α	thermal diffusivity
β	coefficient of thermal expansion
θ	angular coordinate
ν	kinematic viscosity
ξ	logarithmic radial coordinate
ϕ	dimensionless temperature
ψ	dimensionless stream function.

Subscripts

r	radial direction
s	surface condition
θ	transverse direction
∞	free stream condition.

vection flow past a horizontal rod or cylinder immersed in a Newtonian fluid, the corresponding problem of mixed convection in a porous medium has received comparatively much less attention. To the authors' knowledge, only the papers by Cheng [12], Minkowycz *et al.* [13] and Huang *et al.* [14] exist in the literature on the problem of mixed convection past a horizontal cylinder in the presence of boundary-layer flows. Reference [12] reports similarity solutions for the steady mixed convection flow about an isothermal cylinder while in ref. [13] the authors have derived approximate solutions of the boundary-layer equations based on the local similarity and non-similarity methods for the problem of mixed convection from a non-isothermal cylinder. Numerical solutions were carried out up to the third level of truncation. In ref. [14] the authors extended the problem described in ref. [12] to the case of a uniform surface heat flux. The governing boundary-layer equations were solved by employing an implicit finite-difference method. All three papers treated the case of parallel flow only. However, no prior study was done for this problem to investigate the accuracy and limitations of the boundary-layer simplifications as well as the assumptions of potential flow outside the boundary layer. It is, therefore, the aim of this paper to carry out a detailed numerical analysis of the combined convection heat transfer from an isothermal horizontal rod of circular cross-section embedded in a porous medium for the two cases when the forced flow is directed either vertically upward (parallel flow) or vertically downward (counter flow), respectively. We would like to emphasize that the investigation is based on the solution of the full equations of mass, momentum and energy, and not on the boundary-layer equations and so the gravitational force normal to the heated surface of the rod is not neglected. The governing equations were solved using a finite-difference scheme similar to that developed in refs. [15, 16] and applied successfully to some viscous mixed convection problems (non-porous medium) in refs. [17–19]. The velocity and thermal fields are developed in time until reaching the steady-state conditions. The numerical calculations include details of the steady-state flow behaviour as well as results for the local and average Nusselt numbers as a function of both Grashof and Reynolds numbers.

The purpose of the present work is twofold: first to study the case of parallel flow in order to get information concerning the variation of the local and average Nusselt numbers over the rod surface, and second to present results for the case of the counter-flow regime and show the effect of different parameters on streamline and isotherm patterns. In particular, we focus attention on the flow region near the upper and lower stagnation points. Sample results of the heat transfer rate are presented in tables for a range of Reynolds and Grashof numbers. We believe that such tabulations might serve as a reference against which other approximate solutions or experimental data can be compared in the future.

2. BASIC EQUATIONS

Consider a horizontal rod of radius a embedded in a fluid-saturated porous medium of uniform free stream velocity u_∞ and temperature T_∞. The free stream is directed either vertically upward or vertically downward, respectively, as shown in Fig. 1. Let the temperature of the rod be suddenly increased to and maintained at a constant value T_s ($> T_\infty$) for all subsequent times, which will cause transient thermal con-

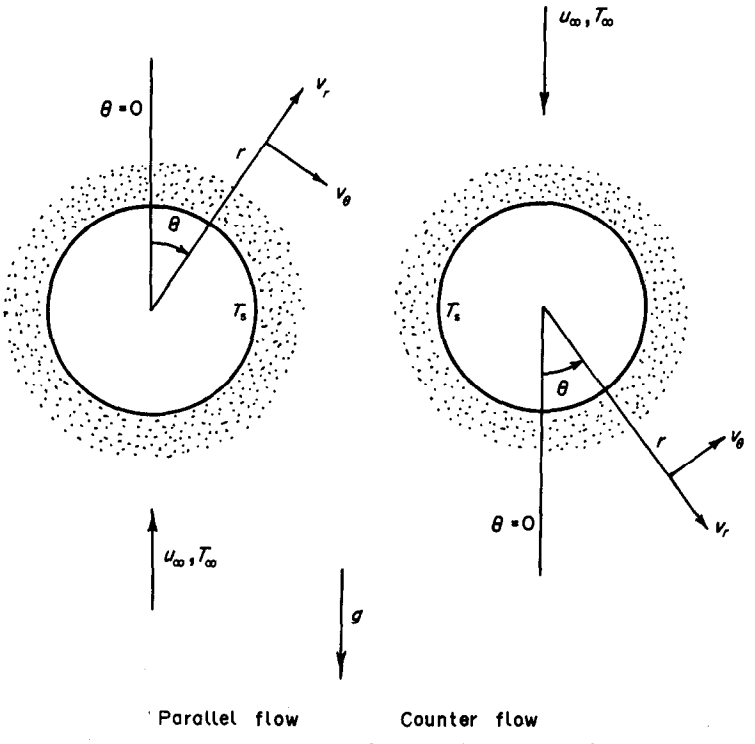

FIG. 1. Coordinate systems for parallel and counter flows.

vection in the medium. The line $\theta = 0°$ is considered to be the radius through the rear-most point on the rod surface viewed from the upstream direction (i.e. the free stream will always be in the direction $\theta = 0°$). In the porous medium, Darcy's law is assumed to hold, the fluid is presumed to be a normal Boussinesq fluid, and the viscous drag and inertia terms of the momentum equations are neglected because their magnitudes are of small order compared to other terms for low Darcy numbers and low particle Reynolds numbers. Owing to the last assumption, velocity slip at the rod surface is permitted.

With these assumptions, the conservation equations for mass, momentum and energy for unsteady flow in an isotropic porous medium can be written in polar coordinates (r', θ) as

$$\nabla'^2\psi' \pm \frac{g\beta K}{\nu}\left(\frac{\partial T}{\partial r'}\sin\theta + \frac{\partial T}{\partial \theta}\frac{\cos\theta}{r'}\right) = 0 \qquad (1)$$

$$\frac{\partial T}{\partial t'} + v_{r'}\frac{\partial T}{\partial r'} + \frac{v_\theta'}{r'}\frac{\partial T}{\partial \theta} = \alpha\nabla'^2 T \qquad (2)$$

where

$$\nabla'^2 = \frac{\partial^2}{\partial r'^2} + \frac{1}{r'}\frac{\partial}{\partial r'} + \frac{1}{r'^2}\frac{\partial^2}{\partial \theta^2}$$

t' is the time, $v_{r'}$ and v_θ' are velocities in the r'- and θ-directions, T the temperature and the other variables are defined in the Nomenclature. The stream function ψ is related to the velocity components by

$$v_r = r'^{-1}\partial\psi'/\partial\theta, \quad v_\theta = -\partial\psi'/\partial r'. \qquad (3)$$

The equations are further transformed to their non-dimensional form by introducing the following dimensionless quantities:

$$t = t'u_\infty/a, \quad r = r'/a, \quad v_r = v_{r'}/u_\infty,$$

$$v_\theta = v_\theta'/u_\infty, \quad \psi = \psi'/au_\infty, \quad \phi = (T - T_\infty)/(T_s - T_\infty).$$

Using the above variables, equations (1) and (2) become

$$\nabla^2\psi \pm \frac{Gr}{Re}\left(\frac{\partial\phi}{\partial r}\sin\theta + \frac{\partial\phi}{\partial\theta}\frac{\cos\theta}{r}\right) = 0 \qquad (4)$$

$$\frac{\partial\phi}{\partial t} + v_r\frac{\partial\phi}{\partial r} + \frac{v_\theta}{r}\frac{\partial\phi}{\partial\theta} = \frac{2}{Re\,Pr}\nabla^2\phi \qquad (5)$$

where

$$Gr = g\beta K(T_s - T_\infty)(2a)/\nu^2$$

is the modified Grashof number

$$Re = 2au_\infty/\nu$$

is the Reynolds number, and

$$Pr = \nu/\alpha$$

is the Prandtl number. It should be noted that the sign of the buoyancy term in equation (4) depends on

the flow regime and is positive for parallel flow and negative for counter flow.

The appropriate boundary conditions of equations (4) and (5) are

$$v_r = 0 \quad \text{and} \quad \phi = 1 \quad \text{at} \quad r = 1 \tag{6a}$$

$$v_r \to \cos\theta, \quad v_\theta \to -\sin\theta, \quad \text{and} \quad \phi \to 0 \quad \text{as} \quad r \to \infty. \tag{6b}$$

In the next section, we rely on a direct numerical solution to determine the basic features of the steady-state mixed convection phenomena taking place in the porous region adjacent to the rod surface.

3. METHOD OF SOLUTION

The governing equations (4) and (5) are solved using essentially the same finite-difference scheme as that described in refs. [17–19]. In this solution method the modified polar coordinates (ξ, θ) are employed, where $\xi = \ln r$ and accordingly the above equations (4) and (5) are transformed to

$$\frac{\partial^2\psi}{\partial\xi^2} + \frac{\partial^2\psi}{\partial\theta^2} \pm e^{\xi}\frac{Gr}{Re}\left(\frac{\partial\phi}{\partial\xi}\sin\theta + \frac{\partial\phi}{\partial\theta}\cos\theta\right) = 0 \tag{7}$$

$$e^{2\xi}\frac{\partial\phi}{\partial t} = \frac{2}{Re\,Pr}\left(\frac{\partial^2\phi}{\partial\xi^2} + \frac{\partial^2\phi}{\partial\theta^2}\right) - \frac{\partial\psi}{\partial\theta}\frac{\partial\phi}{\partial\xi} + \frac{\partial\psi}{\partial\xi}\frac{\partial\phi}{\partial\theta} \tag{8}$$

where the dimensionless radial and transverse velocity components v_r and v_θ become

$$v_r = r^{-1}\,\partial\psi/\partial\theta = e^{-\xi}\,\partial\psi/\partial\theta,$$
$$v_\theta = -\partial\psi/\partial r = -e^{-\xi}\,\partial\psi/\partial\xi. \tag{9}$$

Boundary conditions (6) can be written as

$$\psi = \partial\psi/\partial\theta = 0, \quad \phi = 1 \quad \text{at} \quad \xi = 0 \tag{10a}$$

$$e^{-\xi}\,\partial\psi/\partial\theta \to \cos\theta, \quad e^{-\xi}\,\partial\psi/\partial\xi \to \sin\theta,$$
$$\text{and} \quad \phi \to 0 \quad \text{as} \quad \xi \to \infty. \tag{10b}$$

Since the flow and temperature fields are symmetric about a vertical line passing through the centre of the rod, the following series expansion of the stream function ψ and temperature ϕ is assumed

$$\psi = \sum_{n=1}^{N} f_n(\xi, t)\sin n\theta \tag{11a}$$

$$\phi = \tfrac{1}{2}g_0(\xi, t) + \sum_{n=1}^{N} g_n(\xi, t)\cos n\theta. \tag{11b}$$

The same truncated Fourier series has been used by Ingham *et al.* [11] for studying the free convection limit ($Re = 0$) of the problem. When equations (11) are substituted into equations (7) and (8), and like terms in sin and cos equated, the following differential equations can be deduced:

$$\frac{\partial^2 f_n}{\partial\xi^2} - n^2 f_n \pm S_n = 0 \tag{12a}$$

$$e^{2\xi}\frac{\partial g_0}{\partial t} = \frac{2}{Re\,Pr}\frac{\partial^2 g_0}{\partial\xi^2} + Z_0 \tag{12b}$$

$$2e^{2\xi}\frac{\partial g_n}{\partial t} = \frac{2}{Re\,Pr}\left(\frac{\partial^2 g_n}{\partial\xi^2} - n^2 g_n\right) - nf_n\frac{\partial g_0}{\partial\xi} + Z_n \tag{12c}$$

where S_n, Z_0 and Z_n are functions of ξ and t defined as

$$S_n(\xi, t) = e^{\xi}\frac{Gr}{2Re}\left[-\delta_n\frac{\partial g_0}{\partial\xi} + \frac{\partial g_{n+1}}{\partial\xi} - \frac{\partial g_{n-1}}{\partial\xi} + (n-1)g_{n-1} + (n+1)g_{n+1}\right] \tag{13a}$$

$$Z_0(\xi, t) = -\sum_{n=1}^{N} n\left(f_n\frac{\partial g_n}{\partial\xi} + g_n\frac{\partial f_n}{\partial\xi}\right) \tag{13b}$$

$$Z_n(\xi, t) = -\sum_{m=1}^{N}\left\{\frac{\partial g_m}{\partial\xi}(if_i + jf_j) + mg_m\left[\frac{\partial f_j}{\partial\xi} + \operatorname{sgn}(m-n)\frac{\partial f_i}{\partial\xi}\right]\right\} \tag{13c}$$

where

$$\delta_n = \begin{cases} 1 \text{ for } n = 1 \\ 0 \text{ for } n \neq 1 \end{cases}, \quad i = |m-n|, \quad j = m+n$$

and $\operatorname{sgn}(m-n)$ denotes the sign of the term $(m-n)$.

The appropriate boundary conditions of functions f_n, g_0 and g_n are

$$f_n = g_n = 0 \quad \text{and} \quad g_0 = 2 \quad \text{at} \quad \xi = 0 \tag{14a}$$

$$f_n \to \delta_n e^{\xi}, \quad \partial f_n/\partial\xi \to \delta_n e^{\xi},$$
$$\text{and} \quad g_0, g_n \to 0 \quad \text{as} \quad \xi \to \infty. \tag{14b}$$

For engineering applications, we are often concerned with the effect of fluid motion on the heat transfer from the rod surface. This can be evaluated by computing the local Nusselt number Nu and the mean Nusselt number $\overline{Nu}$ averaged over the rod surface which are given by

$$\left.\begin{aligned} Nu &= 2ah/k \\ \overline{Nu} &= 2a\bar{h}/k \end{aligned}\right\} \tag{15}$$

where h and $\bar{h}$ represent the local and average heat transfer coefficients, which are given by

$$h = q_s/(T_s - T_\infty), \quad \bar{h} = 1/2\pi\int_0^{2\pi} h\,d\theta,$$
$$\text{and} \quad q_s = -k[\partial T/\partial r']_{r'=a} \tag{16}$$

From equations (11), (15) and (16) it follows that the Nusselt numbers can be expressed in the form:

$$Nu = \left[-\frac{\partial g_0}{\partial\xi} - 2\sum_{n=1}^{N}\frac{\partial g_n}{\partial\xi}\sin n\theta\right]_{\xi=0} \tag{17a}$$

$$\overline{Nu} = \left[-\frac{\partial g_0}{\partial\xi}\right]_{\xi=0}. \tag{17b}$$

As mentioned before, a complete numerical solution to equations (12) with boundary conditions (14) is obtained by using a method similar to that given in

refs. [17–19]; its detailed formulation is omitted here since it is well described in the above mentioned references.

4. RESULTS AND DISCUSSION

4.1. *Introductory comments*

The combined convection heat transfer from a horizontal rod embedded in a fluid-saturated porous medium is studied numerically for the two cases when the forced flow is directed either vertically upward (parallel flow) or vertically downward (counter flow). The numerical step-by-step procedure has been performed right up to the steady-state solution and it is shown that this flow is dependent on the Reynolds number, Re, Grashof number, Gr, Prandtl number Pr, in addition to the direction of the forced flow. Moreover, the quantity Gr/Re in equation (4) is a measure of relative importance of free to forced convection, and is one of the controlling parameters for the present problem. For each of the cases considered in this paper, the steady-state regime was achieved after a certain time from the start of the motion. This time varies from one case to another, the maximum time needed being $t = 40$. For all the results which are presented here, the Prandtl number considered is 0.7 but the general ideas hold for other values, too. Let us now discuss the results in each of its two parts of parallel flow and counter flow, respectively.

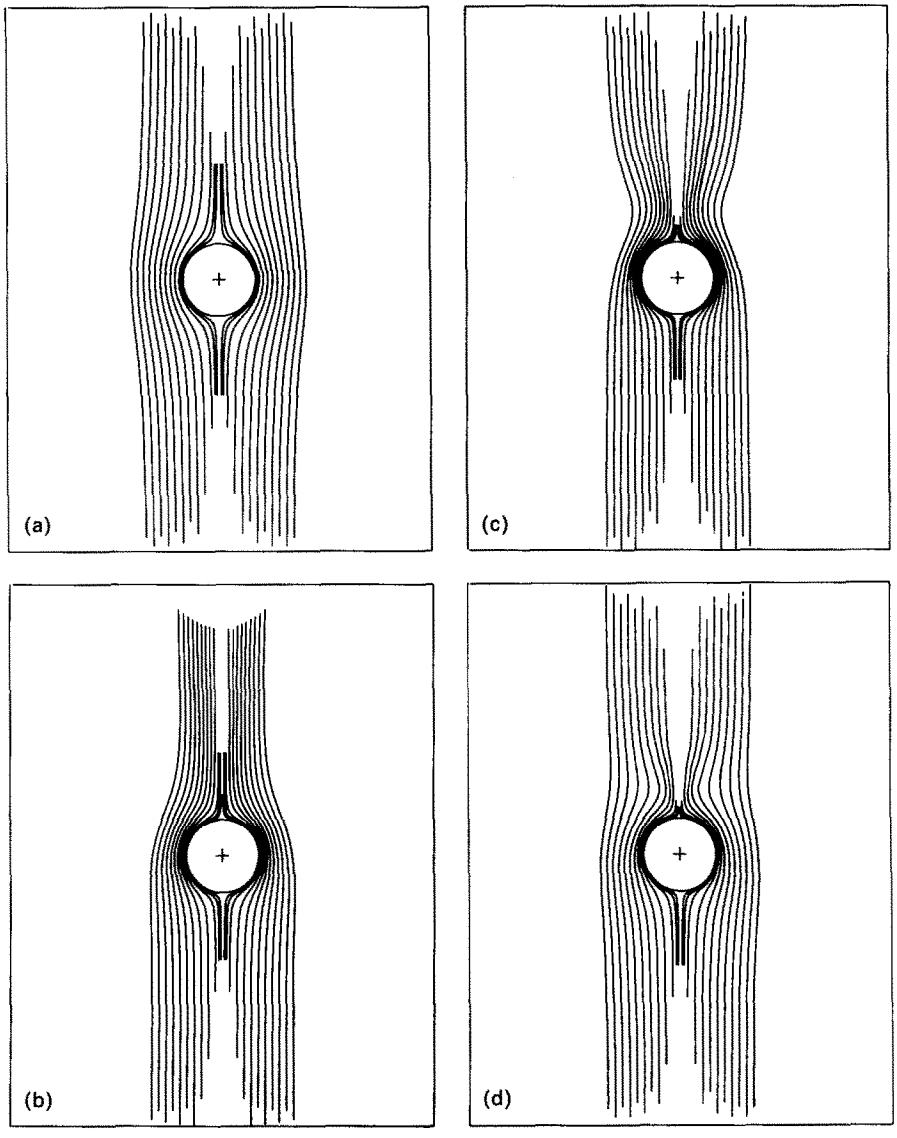

FIG. 2. The streamline pattern for the case of parallel flow: (a) $Re = 20$, $Gr = 0$; (b) $Re = 20$, $Gr = 40$; (c) $Re = 20$, $Gr = 80$; (d) $Re = 100$, $Gr = 400$. Streamlines plotted are $\psi = -2.0, -1.8, -1.6, -1.4, -1.2, -1.0, -0.8, -0.6, -0.4, -0.2, -0.1, -0.05, 0, 0.05, 0.1, 0.2, 0.4, 0.6, 0.8, 1.0, 1.2, 1.4, 1.6, 1.8, 2.0$.

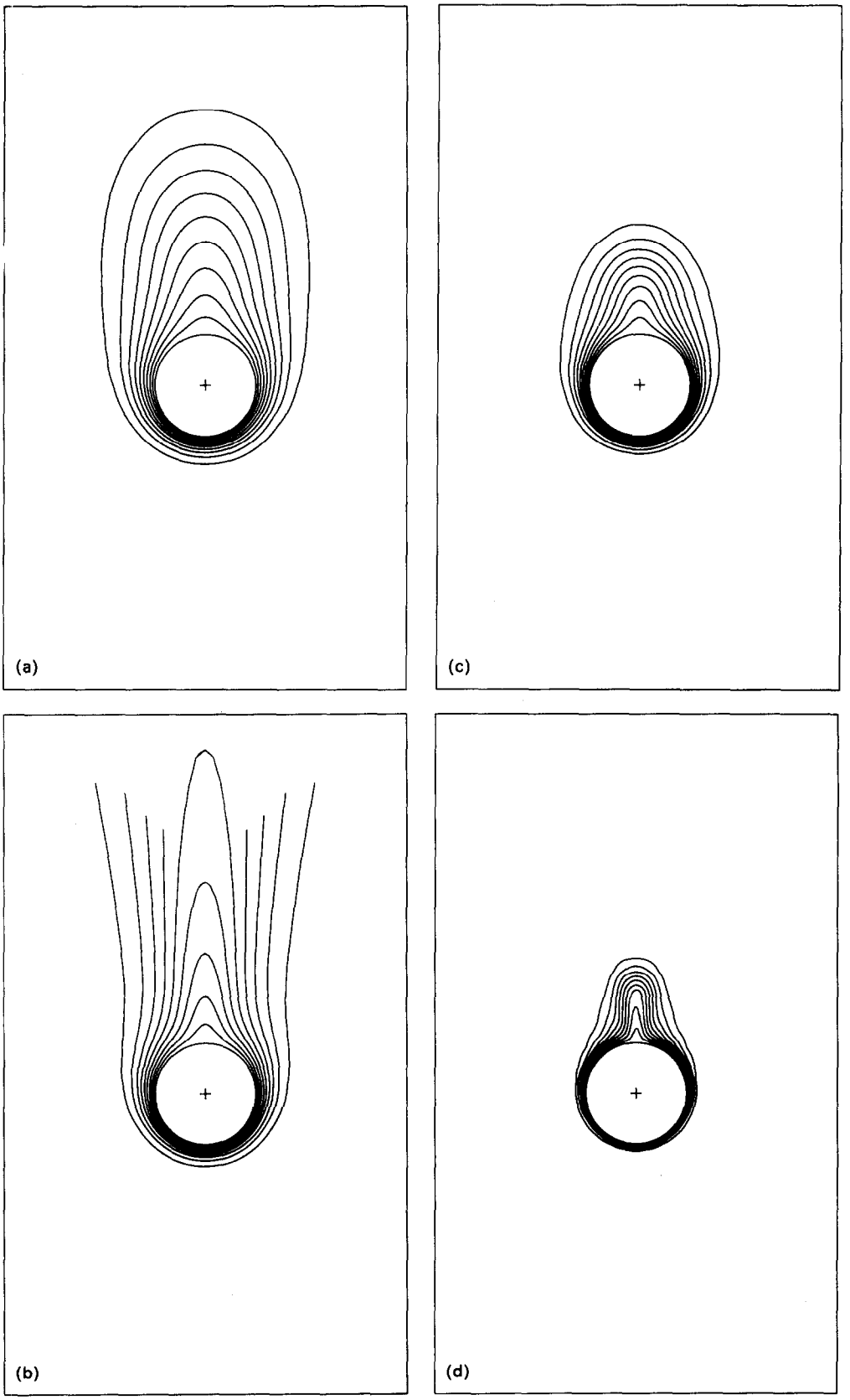

FIG. 3. The isotherm pattern for the case of parallel flow: (a) $Re = 20$, $Gr = 0$; (b) $Re = 20$, $Gr = 40$; (c) $Re = 20$, $Gr = 80$; (d) $Re = 100$, $Gr = 400$. Isotherms plotted are $\phi = 0.1, 0.2, 0.3, \ldots, 0.9$.

4.2. *Parallel flow*

The numerical solution of the steady flow over the rod is obtained for the parallel flow regime at Reynolds numbers of 5, 10, 20, 50 and 100, and for parametric values of the Grashof number in each case. The streamline and isotherm patterns for the cases of $Re = 20$ and 100 and for various values of Gr are presented in Figs. 2(a)–(d) and 3(a)–(d), respectively. We observe from these figures that near the line $\theta = 0°$ a buoyant plume exists above the rod. The width of the plume decreases as Gr increases. The isotherms given in Fig. 3 are seen to be distorted in accordance with the flow patterns. The temperature distribution resembles what would be found near a line heat source where the heat is convected from the rod in a well-defined plume. As Gr becomes larger a thick boundary layer develops around the rod and the $\phi = 0.9$ isotherm gets closer to the rod surface near $\theta = 180°$ as shown in Fig. 3(d). This fact indicates higher temperature gradient and consequently greater heat transfer rates there.

Figures 4(a) and (b) represent the temperature distribution at $\theta = 0°$ as a function of the radial distance r for different values of Gr and for $Re = 10$ and 50. If we consider the forced convection regime ($Gr/2Re = 0$) as the standard case, we first note from Fig. 4(a) that the buoyancy forces increase the temperature along $\theta = 0°$. It is also seen that the temperature decreases almost linearly with the radial distance indicating that conduction is predominant. Then at higher Reynolds numbers ($Re > 50$) Gr has a stronger effect on the temperature distribution. The temperature profiles displayed in Fig. 4(b) for $Re = 50$ are very similar to those predicted by the boundary-layer solution obtained by Minkowycz *et al.* [13]. The same trend is also observed in Figs. 5(a) and (b) as well as in Figs. 6(a) and (b) for the radial and tangential velocity components, the latter being plotted along the radial line $\theta = 90°$ where the tangential component increases greatly close to the surface of the rod.

The calculated values of the average Nusselt number $\overline{Nu}$ are listed in Table 1 from which it can be concluded that $\overline{Nu}$, at a given Re, increases continuously with the increase of Gr. Typical results of the calculations for $\overline{Nu}$ corresponding to $Re = 20$, 50 and 100 are also plotted in Fig. 7 as a function of $Gr/2Re$ (on the right-hand side of this figure). One can see here the gradual increase of $\overline{Nu}$ with the increase in Re.

In Figs. 8(a) and (b), we compare the variation of the local Nusselt number Nu with the angle θ for different Grashof numbers when $Re = 10$ and 50. The numerical solution to the boundary-layer equations obtained by Cheng [12] and Minkowycz *et al.* [13] is also included for comparison. According to ref. [12], the local Nusselt number distribution is given by

$$Nu = 2.828(Pr\,Re)^{1/2} \sin(\theta/2)[-\phi'(0)] \quad (18)$$

where the numerical values of the dimensionless temperature gradient ϕ' are given in ref. [20] for different values of Gr/Re. Figure 8 clearly shows that Nu decreases monotonically from the highest value at $\theta = 180°$ and reaches a minimum at $\theta = 0°$. This behaviour agrees reasonably well, both qualitatively and quantitatively, with the variation of Nu predicted from the boundary-layer solution over all the rod surface except near the top region ($\theta = 0°$). The value of $Nu = 0$ at $\theta = 0°$ obtained from the boundary-layer solution (equation (18)) is questionable since the boundary-layer assumption is no longer valid in the region of the plume. Figure 8(b) shows that the effect of buoyancy forces is predominant for the values of Re and Gr considered. The assumption of negligible curvature effect is not valid at these Grashof numbers, so the solution to the boundary-layer equations only, does not give valid results here. Further, it is relevant to note that the response of Nu to the increase in Re and Gr near $\theta = 0°$ is somewhat different. In this region, Nu changes only slightly with the variation of Re and Gr. A small increase in Gr above its zero value causes a small decrease in Nu at $\theta = 0°$; the values of Nu being smaller than those of the forced convection flow. This is mainly because the buoyancy forces have the least influence at $\theta = 0°$. On the other hand, the initial increase of Gr implies a decrease in the tem-

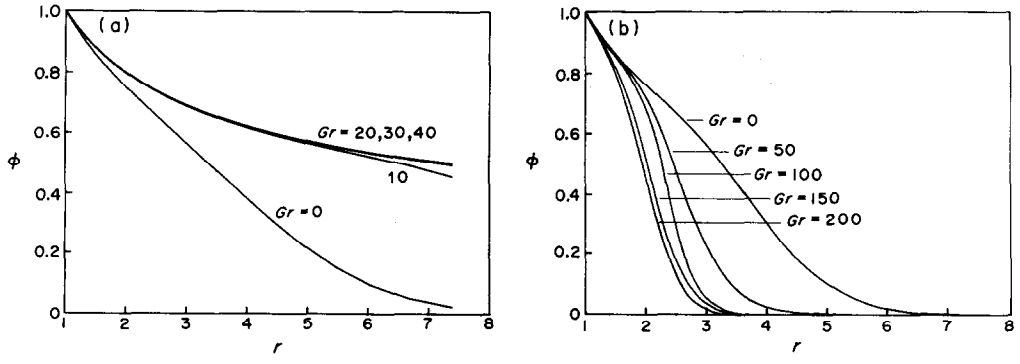

FIG. 4. Variation of the dimensionless temperature in the radial direction at $\theta = 0°$ for the case of parallel flow: (a) $Re = 10$; (b) $Re = 50$.

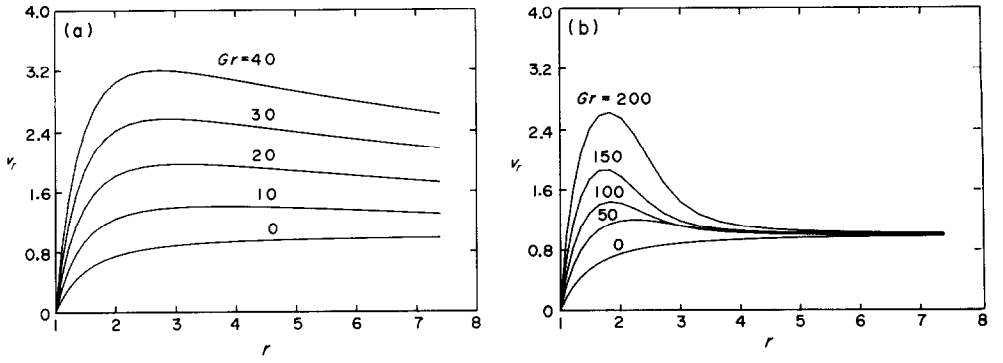

FIG. 5. The radial velocity distribution at $\theta = 0°$ for the case of parallel flow: (a) $Re = 10$; (b) $Re = 50$.

perature gradient at $\theta = 0°$ as Fig 4(a) shows, and accordingly causes a decrease in Nu there.

To this end, we wish to mention that although the results for $Re = 5$ have not been presented in this paper, nevertheless they are consistent in all respects with the general trends outlined above. It may be also opportune to point out here the similarity of these results at moderately large values of Gr with those of Minkowycz *et al.* [13] for the mixed convection boundary-layer flow about a horizontal cylinder buried in a fluid-saturated porous medium. On the other side, the flow characteristics found in this paper are qualitatively similar with those of ref. [17] for the mixed convection flow from a cylinder immersed in an ordinary fluid (without a porous structure).

4.3. *Counter flow*

The second part of this study is devoted to the description of the counter-flow combined convection regime. This is analysed for $Re = 5$, 10, 20, 50 and 100, respectively, and for different values of Gr in each case. The detailed features of the flow and heat transfer for this flow configuration are illustrated in Figs. 9(a)–(f) and 10(a)–(d), where we present results for the streamlines and isotherms at $Re = 5$, 20 and 100, and for different values of Gr. As can be expected on physical grounds, the geometry for the situation of the counter-flow regime is in many respects different from that occurring in the parallel flow case at the same values of Re and Gr. The peculiar behaviour is due to the existence of counter-rotating cells of equal size in each side of the symmetry line $\theta = 0°$. An interesting observation is the shift of these cells toward or above the top region of the rod ($\theta = 180°$) when Gr is increased. The influence of the secondary flow cells on the thermal field is easily observed in Fig. 10 where a considerable distortion of the isotherms takes place especially at high Grashof numbers.

Some of the details of the flow and temperature fields near the rod are presented in Figs. 11–13, where the temperature and velocity profiles are displayed against the radial distance r at different values of Gr and Re. The temperature profiles are plotted for $R = 10$ and 20 while the velocity profiles are traced for $Re = 10$ and 50. It may be seen from Figs. 11(a) and (b) that the effect of increasing Gr is to decrease the temperature gradient at $\theta = 180°$. Furthermore, the profiles gradually change becoming increasingly

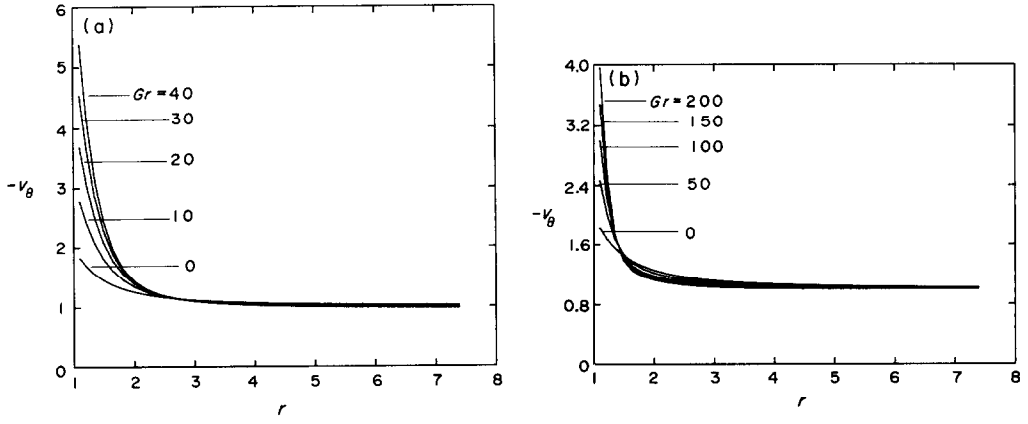

FIG. 6. The tangential velocity variation at $\theta = 90°$ for the case of parallel flow: (a) $Re = 10$; (b) $Re = 50$.

Table 1. Numerical values of the average Nusselt number for the parallel flow regime

Re	$Gr/2Re$	Gr	$\overline{Nu}$
5	0	0	2.032
5	0.5	5	2.314
5	1.0	10	2.639
5	1.5	15	2.948
5	2.0	20	3.238
10	0	0	2.809
10	0.5	10	3.318
10	1.0	20	3.812
10	1.5	30	4.266
10	2.0	40	4.685
20	0	0	3.996
20	0.5	20	4.807
20	1.0	40	5.540
20	1.5	60	5.940
20	2.0	80	6.486
50	0	0	6.604
50	0.5	50	7.896
50	1.0	100	9.008
50	1.5	150	10.018
50	2.0	200	11.003
100	0	0	9.952
100	0.5	100	11.930
100	1.0	200	13.548
100	1.5	300	15.025
100	2.0	400	16.430

steeper as Re gets larger. As Gr increases, the flow field near the rod surface exhibits the formation of two recirculating flow zones where the motion becomes dominated by buoyancy forces. This effect causes the local Nusselt number Nu to increase with the increase of Gr in the region of $\theta = 0°$ while decreasing in the region $\theta = 180°$ as shown in Figs. 14(a) and (b). Also presented in these figures is the boundary-layer solution obtained by using equation (18).

The values of the mean Nusselt number $\overline{Nu}$ were

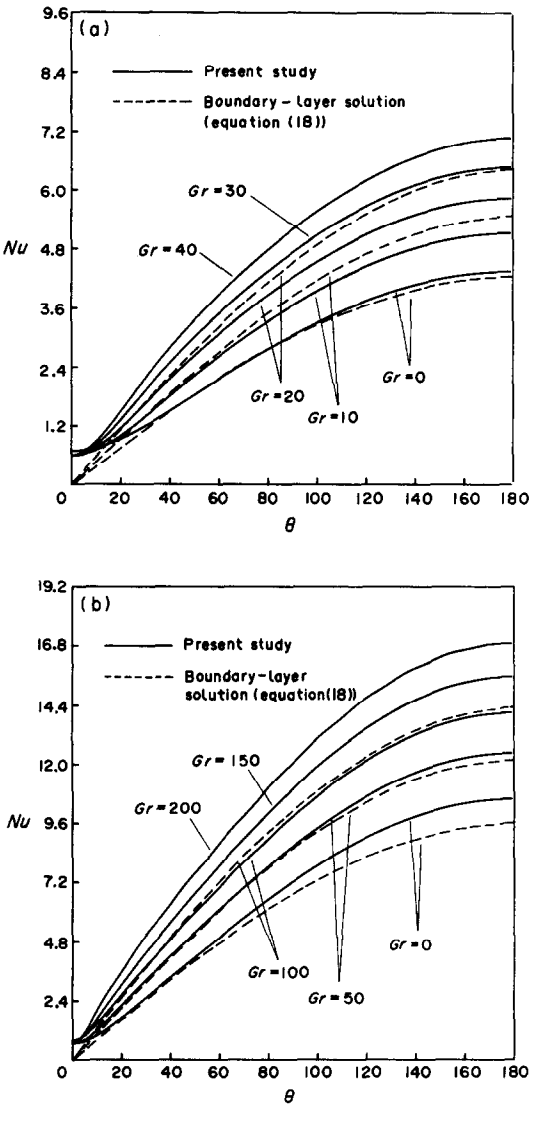

FIG. 8. Variation of the local Nusselt number on the rod surface for the parallel flow: (a) $Re = 10$; (b) $Re = 50$.

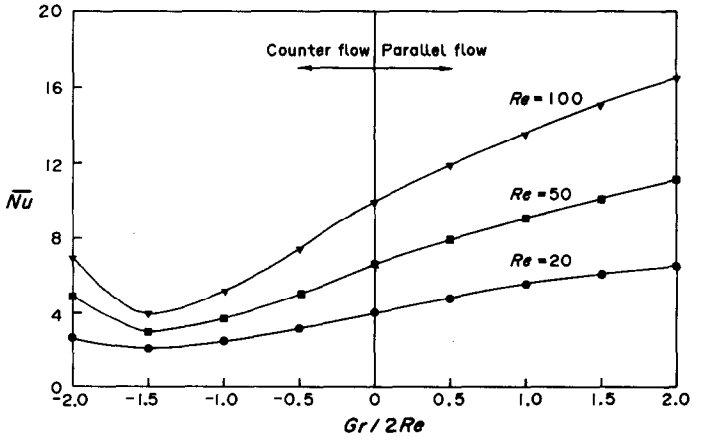

FIG. 7. Variation of the average Nusselt number Nu with $Gr/2Re$ for $Re = 20$, 50 and 100.

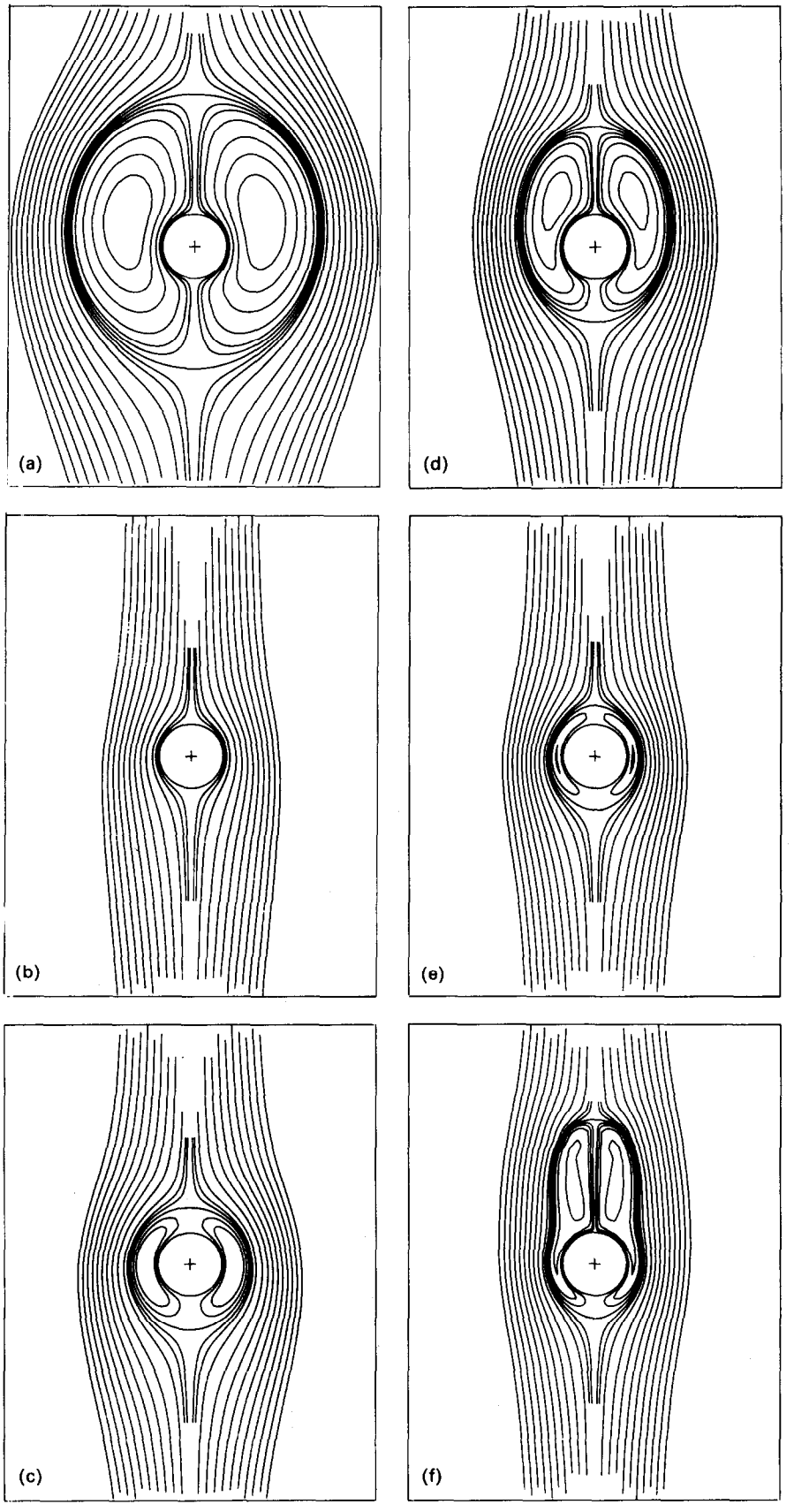

FIG. 9. The streamline pattern for the case of counter flow: (a) $Re = 5$, $Gr = 20$; (b) $Re = 20$, $Gr = 20$; (c) $Re = 20$, $Gr = 60$; (d) $Re = 20$, $Gr = 80$; (e) $Re = 100$, $Gr = 300$; (f) $Re = 100$, $Gr = 400$. Streamlines plotted are the same as in Fig. 2.

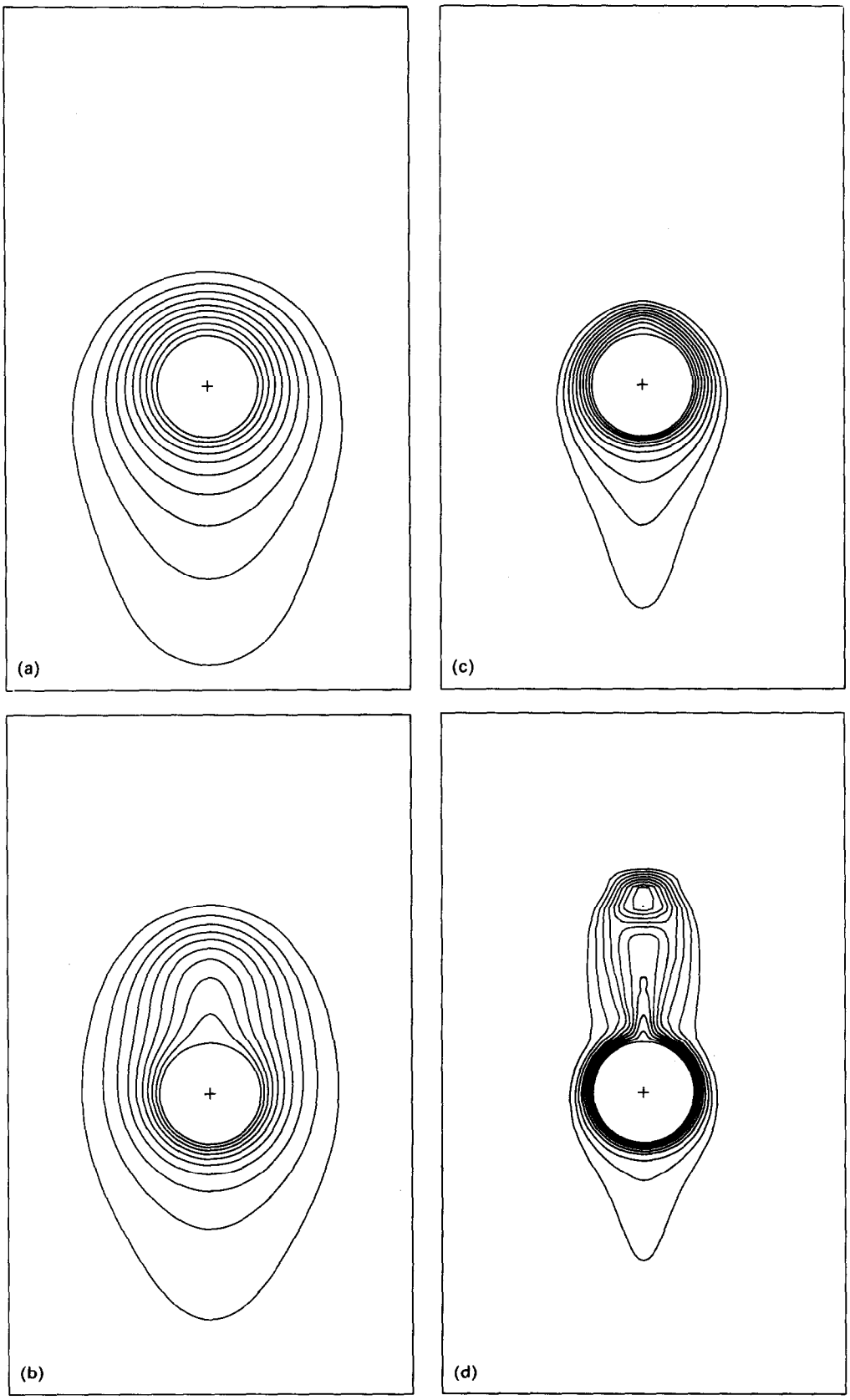

FIG. 10. The isotherm pattern for the case of counter flow: (a) $Re = 20$, $Gr = 60$; (b) $Re = 20$, $Gr = 80$; (c) $Re = 100$, $Gr = 300$; (d) $Re = 100$, $Gr = 400$. Isotherms plotted are the same as in Fig. 3.

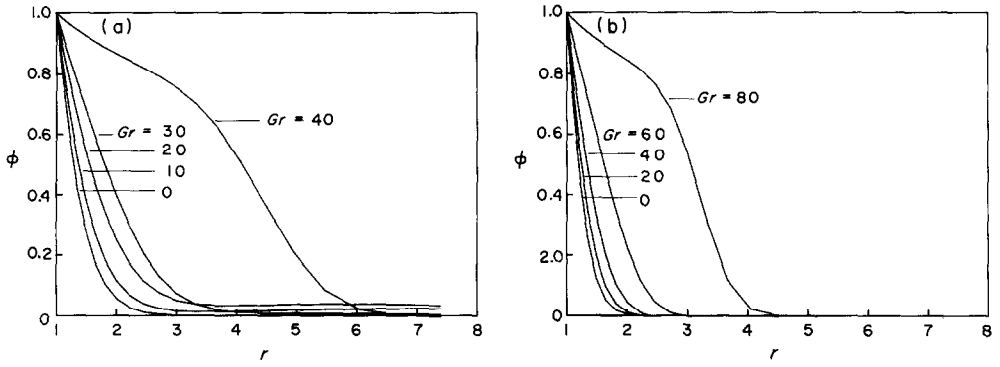

FIG. 11. Variation of the dimensionless temperature in the radial direction at $\theta = 180°$ for the case of counter flow: (a) $Re = 10$; (b) $Re = 20$.

again determined and Table 2 compares the progression of $\overline{Nu}$ with Re and Gr. It is observed from this table that an increase of Gr above its zero value causes a decrease in Nu and this decrease may be considered to be closely related to the secondary flow that occurs near the rod surface. With further increase of Gr, the average Nusselt number increases and hence the flow field becomes more dominated by buoyancy forces. The effects of Re and $Gr/2Re$ on $\overline{Nu}$ for the problem under consideration in this section are again illustrated in Fig. 7 (on the left-hand side of this figure). In contrast to the case of a parallel flow these curves indicate that $\overline{Nu}$ passes through a minimum at $Gr/2Re = 1.5$ for each value of Re considered due to the fact that combined convection becomes less efficient for this value of $Gr/2Re$. However, the maximum value of $\overline{Nu}$ is seen to occur at $Gr = 0$ (forced convection flow) in the considered range of Gr.

5. CONCLUSIONS

Numerical solutions to the complete Darcy and energy equations along with the Boussinesq approximation have been derived for mixed convection heat transfer from an isothermal rod of circular cross-section. In the past, theoretical investigations of mixed convection about horizontal cylinders embedded in porous media were mainly centred upon the boundary-layer approximations. We have presented here results obtained over a wide range of Grashof and Reynolds numbers. The local Nusselt number results are compared with previous published theoretical predictions based on the boundary-layer theory obtained by Cheng [12] and Minkowycz *et al.* [13]. The agreement is good over most of the rod surface except for a small region in the vicinity of $\theta = 0°$ where the boundary-layer approximations are not valid.

In summary, the present study reveals that the

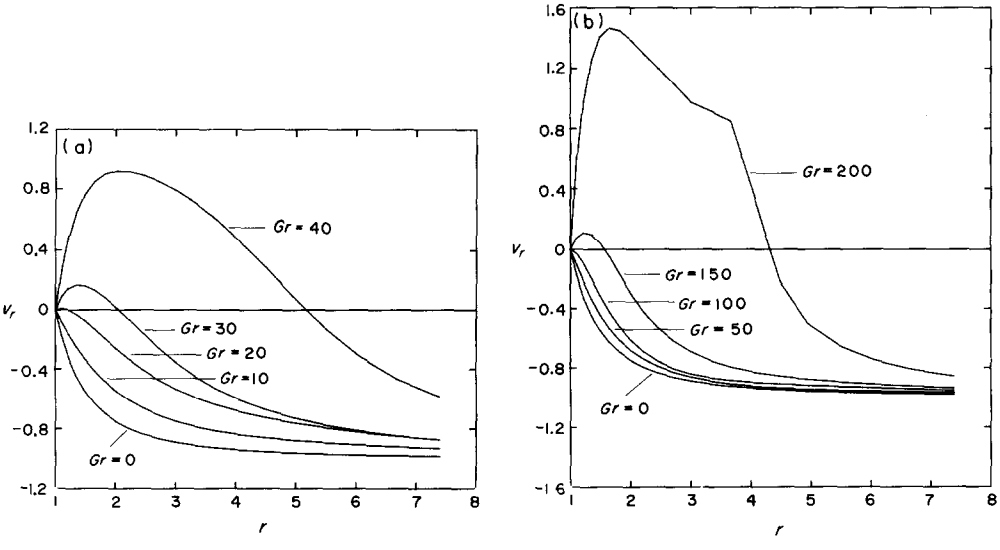

FIG. 12. The radial velocity distribution at $\theta = 180°$ for the case of counter flow: (a) $Re = 10$; (b) $Re = 50$.

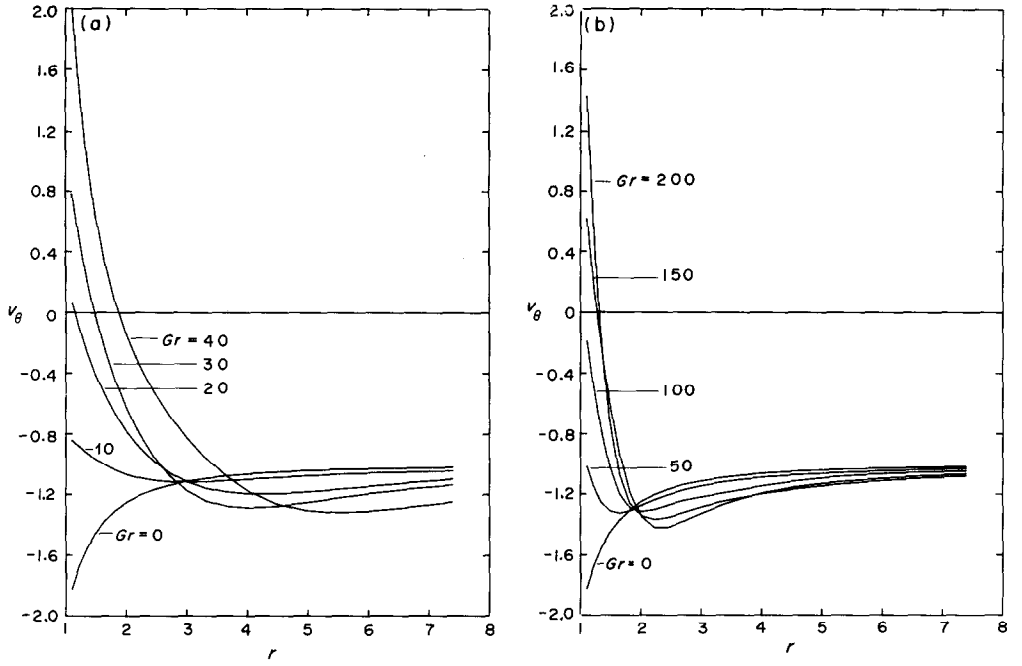

FIG. 13. The tangential velocity variation at $\theta = 90°$ for the counter flow: (a) $Re = 10$; (b) $Re = 50$.

boundary-layer solutions to problems of this type give good results for most practical purposes even at low Grashof numbers. The results show how the theories at both low and high Grashof numbers are approached.

The effects of the interaction between the forced and buoyancy driven flows on the velocity field and heat transfer characteristics are reported and the physics of the mixed convection flow is explained for the two flow configurations of parallel and counter-flow regimes. The method employed works efficiently and quite satisfactorily in analysing the entire flow field including the plume and the recirculating flow zones. Moreover, it is shown that applying such a method to this mixed convection problem not only provides much useful information about the physics of the flow phenomenon but also provides solutions which can be useful in future computational approaches. For

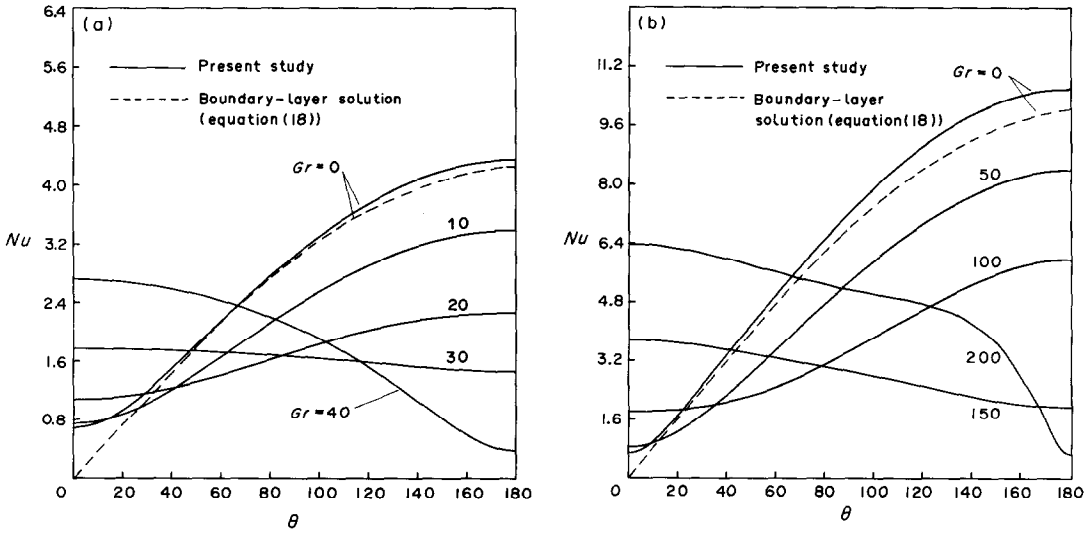

FIG. 14. Variation of the local Nusselt number on the rod surface for the counter flow: (a) $Re = 10$; (b) $Re = 50$.

Table 2. Numerical values of the average Nusselt number for the counter-flow regime

Re	$Gr/2Re$	Gr	$\overline{Nu}$
5	0	0	2.032
5	0.5	5	1.644
5	1.0	10	1.359
5	1.5	15	1.345
5	2.0	20	1.254
10	0	0	2.809
10	0.5	10	2.214
10	1.0	20	1.706
10	1.5	30	1.644
10	2.0	40	1.839
20	0	0	3.996
20	0.5	20	3.140
20	1.0	40	2.430
20	1.5	60	2.060
20	2.0	80	2.700
20	2.5	100	4.100
50	0	0	6.604
50	0.5	50	5.014
50	1.0	100	3.660
50	1.5	150	2.884
50	2.0	200	4.840
100	0	0	9.952
100	0.5	100	7.440
100	1.0	200	5.104
100	1.5	300	3.887
100	2.0	400	6.956

those interested in similar problems, the tabulated data and the accompanied figures provide enough test cases.

Acknowledgements—The financial support of the King Fahd University of Petroleum and Minerals, for H.M.B. during 1986–87 is gratefully acknowledged. The numerous discussions carried out by I.P. with Dr J. H. Merkin (University of Leeds, U.K.) left a considerable imprint on this work. Helpful comments and suggestions have been also made by one of the referees. The authors thank both.

REFERENCES

1. A. Bejan, *Convection Heat Transfer*. Wiley, New York (1984).
2. P. Cheng, Natural convection in a porous medium: external flows. In *Natural Convection: Fundamentals and Applications* (Edited by S. Kakac *et al.*). Hemisphere, Washington, DC (1985).
3. D. A. Nield, Recent research on convection in a porous medium, *Proc. CSIRO/DSIR Seminar on Convective Flows in Porous Media*, D.S.I.R. Wellington, New Zealand (1985).
4. V. E. Schrok, R. T. Fernandez and K. Kesavan, Heat transfer from cylinders embedded in a liquid filled porous medium, *Proc. Int. Heat Transfer Conf.*, Paris-Versailles, Vol. VII, CT-3.6 (1970).
5. R. T. Fernandez and V. E. Schrok, Natural convection from cylinders buried in a liquid-saturated porous medium, *Proc. Int. Heat Transfer Conf.*, Munich, Vol. II, pp. 335–340 (1982).
6. T. Sano, Unsteady heat transfer from a circular cylinder immersed in a Darcy flow, *J. Engng Math.* **14,** 177–190 (1980).
7. J. H. Merkin, Free convection boundary layer on axisymmetric and two-dimensional bodies of arbitrary shape in a saturated porous medium, *Int. J. Heat Mass Transfer* **22,** 1461–1462 (1979).
8. R. H. Nilson, Natural convection boundary layer on two-dimensional and axisymmetric surfaces in high-Pr fluids or in fluid saturated porous medium, *ASME J. Heat Transfer* **103,** 803–807 (1981).
9. R. M. Fand, T. E. Steinberger and P. Cheng, Natural convection heat transfer from a horizontal cylinder embedded in a porous medium, *Int. J. Heat Mass Transfer* **29,** 119–133 (1986).
10. D. B. Ingham and I. Pop, Natural convection about a heated horizontal cylinder in a porous medium, *J. Fluid Mech.* **184,** 157–181 (1987).
11. D. B. Ingham, J. H. Merkin and I. Pop, The collision of free convection boundary layers on a horizontal cylinder embedded in a porous medium, *Q. J. Mech. Appl. Math.* **36,** 313–335 (1983).
12. P. Cheng, Mixed convection about a horizontal cylinder and a sphere in a fluid-saturated porous medium, *Int. J. Heat Mass Transfer* **25,** 1245–1247 (1982).
13. W. J. Minkowycz, P. Cheng and C. H. Chang, Mixed convection about a nonisothermal cylinder and sphere in a porous medium, *Numer. Heat Transfer* **8,** 349–359 (1985).
14. M. J. Huang, K. A. Yih, Y. L. Chou and C. K. Chen, Mixed convection flow over a horizontal cylinder or a sphere embedded in a saturated porous medium, *ASME J. Heat Transfer* **108,** 469–471 (1986).
15. H. M. Badr and S. C. R. Dennis, Unsteady flow past a rotating and translating circular cylinder, *Proc. 8th Canadian Congr. Appl. Mech.*, pp. 659–660 (1981).
16. H. M. Badr and S. C. R. Dennis, Time-dependent viscous flow past an impulsively saturated rotating and translating circular cylinder, *J. Fluid Mech.* **158,** 447–488 (1985).
17. H. M. Badr, A theoretical study of laminar mixed convection from a horizontal cylinder in a cross stream, *Int. J. Heat Mass Transfer* **26,** 639–653 (1983).
18. H. M. Badr, Laminated combined convection from a horizontal cylinder—parallel and contra flow regimes, *Int. J. Heat Mass Transfer* **27,** 15–27 (1984).
19. H. M. Badr, On the effect of flow direction on mixed convection from a horizontal cylinder, *Int. J. Numer. Meth. Fluids* **5,** 1–12 (1985).
20. P. Cheng, Combined free and forced convection flow about inclined surfaces in porous media, *Int. J. Heat Mass Transfer* **20,** 807–815 (1977).

CONVECTION MIXTE AUTOUR D'UNE TIGE HORIZONTALE NOYEE DANS UN MILIEU POREUX

Résumé—Ce papier rapporte les résultats d'une étude numérique du transfert thermique par convection mixte autour d'une tige cylindrique horizontale noyée dans un milieu poreux. La température de la tige est supposée être initialement celle du milieu et portée soudainement à une valeur constante plus élevée. Le problème de régime permanent a été résolu par la méthode de troncature de série en combinaison avec un schéma aux différences finies pour les deux configurations de régime cocourant et contrecourant. Les champs de vitesse et de température et les variations de flux thermique moyens et locaux pour un large domaine des nombres de Reynolds, de Grashof et de paramètre de flottement sont considérés en détail pour un nombre de Prandtl de 0,7. Une des configurations intéressantes trouvées est la possibilité d'un écoulement de recirculation près de la demi-surface supérieure de la tige dans le cas du régime à contre-courant. La méthode numérique et les résultats présentés concernent un manque dans la littérature sur l'un des problèmes les plus fondamentaux dans le domaine de la convection mixte dans un milieu poreux.

GEMISCHTE KONVEKTION AN EINEM ISOTHERMEN, HORIZONTALEN, IN EIN PORÖSES MEDIUM EINGEBETTETEN STAB

Zusammenfassung—In diesem Beitrag wird über die Ergebnisse einer numerischen Untersuchung der Wärmeübertragung durch gemischte Konvektion an einem horizontalen rotationssymmetrischen Stab, der in ein poröses Medium eingebettet ist, berichtet. Es wird zunächst angenommen, daß die Stabtemperatur gleich derjenigen des Mediums ist und dann plötzlich auf einen konstanten höheren Wert verändert wird. Das stationäre Problem wurde mit einer Reihenentwicklung in Kombination mit einem Finite-Differenzen-Verfahren sowohl für Gebiete mit paralleler Strömung als auch für solche mit Gegenströmung gelöst. Sowohl die Strömungs- und Temperaturfelder als auch die Veränderung der mittleren und lokalen Wärmeübergangskoeffizienten wurden in einem großen Bereich von Reynolds-Zahl, Grashof-Zahl und Auftriebsparametern für eine Prandtl-Zahl von 0,7 detailliert untersucht. Eine der interessanten zu beobachtenden Erscheinungen in Bereichen mit Gegenströmung ist das Auftreten einer Rückströmungszone an der oberen Hälfte der Staboberfläche. Das numerische Verfahren und die vorgestellten Ergebnisse füllen eine Lücke in der Literatur für eines der grundlegendsten Probleme auf dem Gebiet der gemischten Konvektion in porösen Medien.

СМЕШАННАЯ КОНВЕКЦИЯ ОТ ИЗОТЕРМИЧЕСКОГО ГОРИЗОНТАЛЬНОГО СТЕРЖНЯ, ПОМЕЩЕННОГО В ПОРИСТУЮ СРЕДУ

Аннотация—Приводятся результаты численного исследования теплопереноса при смешанной конвекции от горизонтального стержня круглого сечения, помещенного в пористую среду. Предполагается, что вначале стержень имеет ту же температуру, что и пористая среда, а затем мгновенно нагревается до более высокой постоянной температуры. Стационарная задача решается методом усечения рядов в комбинации с использованием конечно-разностной схемы для двух конфигураций потока при спутном и встречном режимах течения. Для числа Прандтля, равного 0.7, подробно исследовались динамические и температурные поля, изменение средних и локальных интенсивностей теплопереноса в широких диапазонах чисел Рейнольдса и Грасгофа, а также параметра плавучести. Одним из интересных результатов работы явилось то, что вблизи верхней половины стержня во встречном режиме течения возникает рециркуляционная зона. Численный метод и представленные результаты заполняют имеющийся в литературе пробел по одной из основных проблем в области смешанной конвекции в пористых средах.